

LLM4WM: Adapting LLM for Wireless Multi-Tasking

Xuanyu Liu, Shijian Gao, *Member, IEEE*, Boxun Liu, *Graduate Student Member, IEEE*,
Xiang Cheng, *Fellow, IEEE*, Liuqing Yang, *Fellow, IEEE*

Abstract—The wireless channel is fundamental to communication, encompassing numerous tasks collectively referred to as channel-associated tasks. These tasks can leverage joint learning based on channel characteristics to share representations and enhance system design. To capitalize on this advantage, LLM4WM is proposed—a large language model (LLM) multi-task fine-tuning framework specifically tailored for channel-associated tasks. This framework utilizes a Mixture of Experts with Low-Rank Adaptation (MoE-LoRA) approach for multi-task fine-tuning, enabling the transfer of the pre-trained LLM’s general knowledge to these tasks. Given the unique characteristics of wireless channel data, preprocessing modules, adapter modules, and multi-task output layers are designed to align the channel data with the LLM’s semantic feature space. Experiments on a channel-associated multi-task dataset demonstrate that LLM4WM outperforms existing methodologies in both full-sample and few-shot evaluations, owing to its robust multi-task joint modeling and transfer learning capabilities.

Index Terms—large language models, Mixture of Experts, Low-Rank Adaptation, multi-task learning, wireless multi-tasking, transfer learning.

I. INTRODUCTION

THE wireless channel plays a critical role in determining the quality and reliability of communication. To achieve the low latency and high reliability required for these applications, millimeter-wave (mmWave) and Multiple-Input Multiple-Output (MIMO) technologies are among the most promising solutions [1]–[3]. Accurate channel estimation is vital for maximizing the benefits of these technologies [4]. However, this task becomes increasingly challenging as the number of antennas grows and environmental dynamics become more complex. Understanding the wireless channel’s characteristics—such as fading, interference, and multipath propagation—is crucial for optimizing performance. Fortunately, artificial intelligence (AI) has significantly improved channel estimation accuracy, fostering optimism for the practical implementation of advanced wireless applications [5]–[7]. AI also enhances various communication tasks, including channel prediction, beamforming, and positioning, demonstrating notable effectiveness and robustness.

Although AI has demonstrated significant potential in communication systems, existing AI-powered communication methods still encounter several issues. First, AI approaches often require large amounts of high-quality data, and collecting such datasets can impose substantial communication overhead on the system. Additionally, due to generalization issues, AI

models need to be retrained in response to dynamic changes in the environment, further increasing the communication burden. Furthermore, existing AI methods frequently struggle in complex and highly dynamic scenarios, often due to the limited scale of the models.

To address these challenges, [8] proposed that multi-modal sensing could effectively capture the propagation characteristics of the wireless channel, a concept summarized as the Synesthesia of Machines (SoM). This approach aims to optimize communication systems by leveraging multi-modal sensing to enhance their design and performance [9], [10].

Another potential optimization approach is the introduction of multi-task learning. Given that the wireless channel is a critical component of the wireless communication process, and many communication tasks focus on the extraction and utilization of channel features under various conditions, jointly learning these channel-associated tasks can yield significant training benefits by extracting shared channel representations across tasks. For instance, in [11], two key tasks of wireless signal recognition—signal classification and modulation recognition—were jointly trained. In [12], the joint training and inference of direct channel and cascaded channel estimation in reconfigurable intelligent surface systems were proposed, effectively reducing pilot overhead. Despite their effectiveness, these methods have limitations, such as issues with data imbalance and the seesaw effect in multi-task learning approaches that rely on shared representations at the bottom layers. Additionally, challenges arise in scaling the number and diversity of tasks due to limited model capacity, as most methods combine only two closely related tasks.

Recently, large language models (LLMs) have emerged as powerful multi-task learners, demonstrating remarkable reasoning capabilities and generalization across various domains, including natural language processing (NLP) [13], healthcare [14], law [15], and finance [16]. The GPT-4 has shown outstanding performance in NLP tasks, while models like BeiT [17] have achieved state-of-the-art results in computer vision tasks such as object detection and semantic segmentation. Inspired by these successes, there is growing interest in leveraging pre-trained models for cross-domain tasks, including channel-associated tasks in wireless communication. For instance, an LLM-empowered channel prediction method LLM4CP was proposed in [18], achieving greatly improved few-shot generalization ability. A foundational channel model WiFo [19] was trained on a diverse channel dataset to perform tasks like time-domain and frequency-domain prediction with zero-shot learning, but they primarily focus on channel

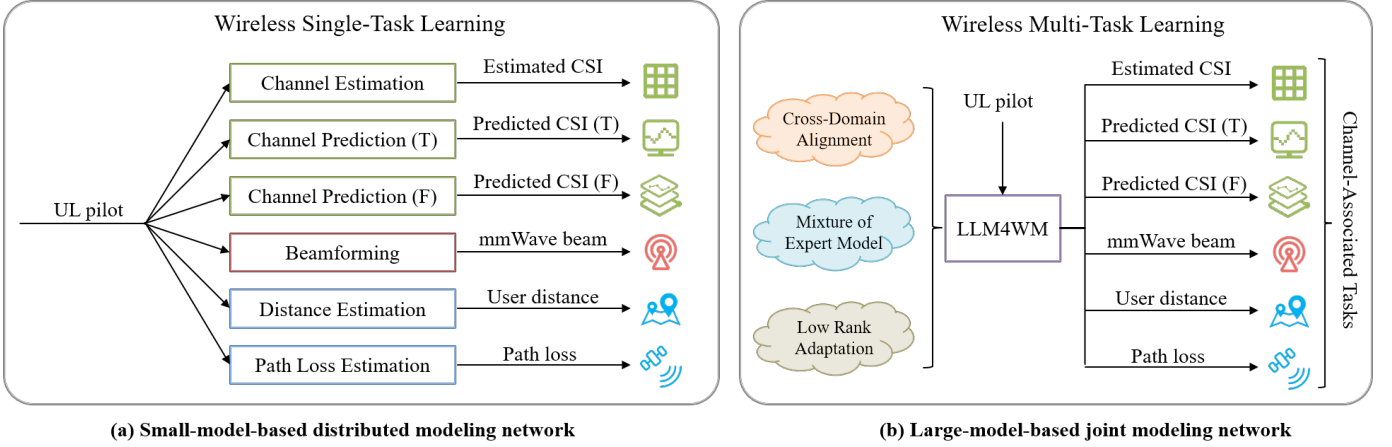


Fig. 1. An illustration highlighting the differences in the workflows between a small-model-based distributed modeling and a large-model-based joint modeling.

reconstruction. Our objective is to enhance multiple channel-associated tasks in wireless communication using LLMs, which poses challenges such as effectively transferring cross-domain knowledge and managing task diversity. We address these challenges through the MoE-LoRA fine-tuning method [20], designed for multi-task scenarios, while noting that recent work has not sufficiently considered the specific relationships between channel-associated tasks, potentially hindering the model’s ability to learn general representations.

Specifically, we propose a multi-task fine-tuning framework based on pre-trained large language models, which is successfully applied to the channel-associated multi-tasks. Unlike previous multi-task learning approaches that rely on shared bottom layers, we freeze most of the large model’s parameters and introduce MoE-LoRA for multi-task fine-tuning. On the one hand, tasks can share experts’ weight, which helps the network learn common knowledge across tasks, while on the other hand, the independence of experts and the gating mechanism ensure the differentiation of task-specific features. Additionally, we incorporate multi-task adapter modules at both the input and output layers of the LLM to ensure alignment between the feature space of communication tasks and the semantic feature space of the model. To further enhance our framework, we also design a pre-processing method and corresponding output header for each task, which optimizes the overall performance and adaptability of the model. The key contributions of our work are summarized as follows:

- LLM4WM is introduced as a novel method that leverages LLM to facilitate wireless multi-tasking. This approach represents a pioneering effort in fine-tuning LLM using MoE-LoRA to extract a joint representation tailored for wireless multi-task scenarios, establishing a new standard in this area of research.
- To ensure effective cross-domain alignment, a customized pre-processing method and corresponding output header have been developed for each task. Additionally, multi-task adapters are created to bridge the gap between the LLM’s semantic feature space and the specific feature space of wireless tasks, enhancing adaptability and performance.

- The model demonstrates strong performance across a variety of tasks, including channel estimation, channel prediction, localization enhancement, and beam management. Furthermore, it exhibits impressive generalization capabilities, highlighting robustness and versatility for diverse applications in the wireless domain.

Notation: $(\cdot)^H$, $|\cdot|$ and $\|\cdot\|$ denote the conjugate transpose, determinant and l_2 norm, respectively. $\mathbf{a}[i]$ is the i -th element of a vector \mathbf{a} and $M[i, j]$ denotes the element of matrix or tensor M at the i -th row and the j -th column. The slicing operation $M[s_1 : e_1 : i_1, s_2 : e_2 : i_2]$ is used to extract a submatrix or sub-tensor from M . Here, s_1 and s_2 represent the starting indices, e_1 and e_2 denote the ending indices, and i_1 and i_2 are the step sizes that determine the interval between selected indices. If either i_1 or i_2 equals 1, the step size can be omitted for simplicity. $\mathbb{E}\{\cdot\}$ denotes the statistical expectation of the enclosed variable or expression.

II. SYSTEM DESCRIPTION

A dual-frequency communication system operating at sub-6G and mmWave frequencies is considered, which consists of one base station (BS) and one user equipment (UE). Both the BS and UE utilize multiple-input multiple-output (MISO) and orthogonal frequency division multiplexing (OFDM) technologies, with each equipped with transceivers for both frequency bands. The sub-6G and mmWave antennas are co-located and aligned, with similar apertures, enabling them to share spatial features. For clarity, we use (\cdot) notation, such as \tilde{x} to denote parameters related to the sub-6G system. In mmWave band, the BS adopts an analog beamforming architecture and is equipped with N_t uniform linear array (ULA) antennas, while in the sub-6G band, it utilizes a fully digital beamforming architecture with \tilde{N}_t ULA antennas. The UE is equipped with an omnidirectional antenna for both frequency links and can accommodate multiple antennas through parallel processing. While the analysis assumes line-of-sight (LoS) conditions for both low-frequency and mmWave channels, the proposed scheme can be easily adapted for scenarios with multiple dominant paths.

A. Channel Model

For both sub-6G and mmWave channels, the classical cluster-based multipath channel model is utilized to describe the downlink and uplink CSI between the BS and user at time t and frequency f :

$$\mathbf{h}(t, f) = \sum_{n=1}^N \sum_{m=1}^{M_n} \beta_{n,m} e^{j[2\pi(v_{n,m}t - f\tau_{n,m}) + \Phi_{n,m}]} \mathbf{a}(\theta_{n,m}). \quad (1)$$

In this context, N and M_n are the number of clusters and paths in each cluster, respectively. $\beta_{n,m}$, $v_{n,m}$, $\tau_{n,m}$, and $\Phi_{n,m}$ represent the complex path gain, doppler frequency shift, delay, and random phase, respectively. $\mathbf{a}(\theta_{n,m})$ represents the steering vector of the corresponding path, where $\theta_{n,m}$ denote the azimuth angles of departure (AoD). Considering the structural characteristics of ULA, the expression for $\mathbf{a}(\theta_{n,m})$ is derived as:

$$\mathbf{a}(\theta_{n,m}) = [1, e^{j\frac{2\pi f d_v \sin(\theta_{n,m})}{c}}, \dots, e^{j\frac{2\pi(N_v-1) f d_v \sin(\theta_{n,m})}{c}}]. \quad (2)$$

Here, d_v represents the antenna spacing in the vertical direction.

B. Signal Model

For the mmWave links, We consider a downlink MISO-OFDM signal transmission process, where K subcarriers are activated, with the k -th subcarrier denoted as f_k . According to Eq. (1), the downlink CSI at time t and the k -th subcarrier is $\mathbf{h}_{t,k} = \mathbf{h}(t, f_k)$, which can be obtained through channel estimation or prediction. Considering transmit precoding at the BS side, the received downlink mmWave signal of the time t and k -th subcarrier at the user side is derived as:

$$\mathbf{y}_{t,k} = \mathbf{h}_{t,k}^H \mathbf{w}_t x_{t,k} + \mathbf{n}_{t,k}, \quad (3)$$

where $\mathbf{n}_{t,k}$ is the additive white gaussian noise (AWGN) and $\mathbf{w}_t \in \mathbb{R}^{N_v \times 1}$ is the beam vector which is selected from predefined codebooks \mathcal{W} , i.e. $\mathbf{w}_t \in \mathcal{W}$. The achievable spectral efficiency (SE) [21] of the downlink transmission process is derived as:

$$R_t = \sum_{k=1}^{K_s} \log_2 \left(1 + \frac{|\mathbf{h}_{t,k}^H \mathbf{w}_t|^2}{\sigma_n^2} \right). \quad (4)$$

Through beam training, all beam vectors are traversed from the codebook, and the one with the highest SE is selected as the optimal beam vector, which can be formulated as:

$$\mathbf{w}_t^* = \arg \max_{\mathbf{w}_t \in \mathcal{W}} R_t. \quad (5)$$

Similarly, the sub-6G downlink signal transmission process also adopts MISO-OFDM, and it has the same transmission expression as the mmWave link, which will be omitted here for brevity. However, the sub-6G link employs digital precoding, so the LS method estimates the channel at the pilot positions to get the uplink channel as follows:

$$\tilde{\mathbf{h}}_{LS}(t, f_k) = \tilde{\mathbf{y}}_{t,k} / \tilde{x}_{t,k}, \quad (6)$$

where $\tilde{x}_{t,k}$ and $\tilde{y}_{t,k}$ represent the uplink pilot signal sent by the user and the signal received by the base station respectively.

Then to maximize the system SE, the matched filtering based precoding is applied as follows:

$$\tilde{\mathbf{w}}_{t,k}^* = \frac{\tilde{\mathbf{h}}_{LS}(t, f_k)}{\|\tilde{\mathbf{h}}_{LS}(t, f_k)\|}, \quad (7)$$

where $\tilde{\mathbf{w}}_{t,k}^*$ represents the beam vectors of time t and the k -th subcarrier at sub-6G link. It is worth noting that the effectiveness of $\tilde{\mathbf{w}}_{t,k}^*$ depends on the accuracy of $\tilde{\mathbf{h}}_{LS}(t, f_k)$. Specifically, inaccurate $\tilde{\mathbf{h}}_{LS}(t, f_k)$ will lead to mismatched $\tilde{\mathbf{w}}_{t,k}^*$ with the actual $\tilde{\mathbf{h}}(t, f_k)$, reducing the received signal-to-noise ratio (SNR) and thereby impairing the SE. Therefore, accurate CSI is crucial for improving the SE of the system.

III. TASK DESCRIPTION

To achieve higher SE in the sub-6G frequency band, accurate channel matrix estimation from pilot signals is essential [5]. Research has focused on enhancing pilot-based channel estimation for massive antenna arrays and addressing channel aging in high mobility scenarios through time-domain prediction [22]. Additionally, some studies reduce pilot overhead by extrapolating in the frequency domain [23]. In the mmWave frequency band, the increased number of antennas necessitates improved beam scanning efficiency. Researchers utilize the spatial correlation between frequency bands to estimate optimal mmWave beams based on the sub-6G channel matrix [24]. Parameters like user distance x_d and path loss x_{pl} are also critical for configuring communication links, with some works estimating these factors from channel data [25], [26]. Although the objectives and optimization methods of these tasks differ, they all leverage characteristics of sub-6 GHz channels. Moreover, base stations often need to perform these tasks simultaneously for efficient communication system operation. Thus, designing a unified network to address these tasks concurrently is essential.

We categorize these tasks into three classes: channel reconstruction, beam management, and radio environment mining. To enhance clarity and understanding, we define $\mathcal{T} = \{CE, CP, PF, BF, DE, PE\}$ as the task set. The detailed descriptions are presented in Tab. I.

TABLE I
DESCRIPTION AND CLASSIFICATION OF TASK ID

Task class	Task id	Task content
Channel Reconstruction	CE	Channel estimation
	CP	Temporal domain channel prediction
	PF	Frequency domain channel prediction
Beam Management	BF	Sub-6G assisted mmWave beamforming
Radio Environment Mining	DE	Distance estimation
	PE	Path loss estimation

Each task corresponds to a dataset $D_n = \{X_n^I, X_n^L\}$, where X_n^I represents the input samples for the task n and X_n^L

represents the labels for the task n . All tasks can be formulated in the following form:

$$\max_{\Omega_n} \text{Score}_n = \mathbb{E} \{ f_{eval_n}(\mathbf{X}_n^L, \mathbf{X}_n^O) \} \quad (8a)$$

$$s.t. \quad \mathbf{X}_n^O = f_{\Omega_n}(\mathbf{X}_n^I), \quad n \in \mathcal{T}, \quad (8b)$$

where f_{eval_n} and f_{Ω_n} are the evaluation function and the constructed mapping function for the task n , respectively. \mathbf{X}_n^O represent the output results of the model for the task n . Fig. 1 illustrates the complete workflow of the system. Detailed descriptions of the specific sub-tasks will follow.

A. Channel Reconstruction: Interpolation and Prediction

The objective of channel reconstruction tasks is typically to utilize known channel matrices for the prediction or interpolation of the target channel matrix in the time-frequency domain. The model should learn the inter-domain correlations of the channel matrix across the time, frequency, and antenna domains. So the channel matrix \mathbf{H} considered herein includes three dimensions: time, space, and antenna, and can be expressed as follows:

$$\mathbf{H}[i, j, :] = h(i\Delta t, f_1 + (j-1)\Delta f), \quad (9)$$

where Δt , Δf , and f_1 denote the time interval, frequency interval, and the lowest frequency point in the frequency domain, respectively.

For the channel estimation task, a comb-type pilot pattern is utilized, featuring continuous pilots in the time-domain resource blocks (RBs) and discrete distribution in the frequency-domain RBs. The network must learn channel characteristics across various frequency points and fill in the missing channels at absent frequency points. Consequently, \mathbf{X}_{CE}^I and \mathbf{X}_{CE}^L are defined as follows:

$$\mathbf{X}_{CE}^I = \mathbf{H}[1 : \tilde{T}, 1 : \tilde{K}/n_{pilot} : \tilde{K}, 1 : \tilde{N}_t] \quad (10a)$$

$$\mathbf{X}_{CE}^L = \mathbf{H}[1 : \tilde{T}, 1 : \tilde{K}, 1 : \tilde{N}_t]. \quad (10b)$$

Here, \tilde{T} and \tilde{K} denote the total number of timestamps and the number of OFDM symbols. n_{pilot} denotes the number of pilots, which is typically set such that $\tilde{K}/n_{pilot} = 4$.

For the channel prediction task, we considered two scenarios: time-domain prediction and frequency-domain prediction, both of which help reduce the overhead of pilots. \mathbf{X}_{CP}^I and \mathbf{X}_{CP}^L for the time-domain prediction task are defined as:

$$\mathbf{X}_{CP}^I = \mathbf{H}[1 : \tilde{T}, 1 : \tilde{K}, 1 : \tilde{N}_t] \quad (11a)$$

$$\mathbf{X}_{CP}^L = \mathbf{H}[\tilde{T} + 1 : \tilde{T} + \tilde{P}, 1 : \tilde{K}, 1 : \tilde{N}_t], \quad (11b)$$

where \tilde{P} represents the length of future moments to be predicted. Similarly, for the frequency-domain prediction task, \mathbf{X}_{PF}^I and \mathbf{X}_{PF}^L are defined as:

$$\mathbf{X}_{PF}^I = \mathbf{H}[1 : \tilde{T}, 1 : \tilde{K}/2, 1 : \tilde{N}_t] \quad (12a)$$

$$\mathbf{X}_{PF}^L = \mathbf{H}[1 : \tilde{T}, \tilde{K}/2 : \tilde{K}, 1 : \tilde{N}_t]. \quad (12b)$$

B. Beam Management: Sub-6G Aided Beamforming

Beamforming requires accurate acquisition of the optimal weight vector \mathbf{w}_t based on the codebook $\mathbf{W} \in \mathbb{R}^{N_v \times N_c}$, where N_c is the codebook size. To achieve higher spatial resolution, a super-resolution Discrete Fourier Transform (DFT) codebook is applied, which implies that $N_c > N_v$. Given that the main paths in sub-6G and mmWave bands are often highly correlated in the LoS conditions, utilizing sub-6 GHz to assist mmWave beamforming is highly meaningful. The model extracts the main path information from the sub-6 GHz channel matrix and serves mmWave beamforming, thus the I_{BF} and L_{BF} for sub-6G aided beamforming task can be defined as:

$$\mathbf{X}_{BF}^I = \mathbf{H}[1, 1 : \tilde{K}, 1 : \tilde{N}_t] \quad (13a)$$

$$\mathbf{X}_{BF}^L = \mathbf{w}_t^*. \quad (13b)$$

C. Radio Environment Mining: Distance Estimation and Path Loss Estimation

Due to the rich environmental information contained in the acquired channel data, such as the multipath components reflecting the density of surrounding buildings, and the delay indicating the distance to the target, the task of radio environment mining aims to leverage the estimated channel to extract environmental information, such as the distance x_d between the UE and the BS and the path loss x_{pl} of the main path. This extracted information can be utilized to adjust the configuration of the communication system, ultimately improving communication quality. Thus, \mathbf{X}_{DE}^I and \mathbf{X}_{DE}^L for distance estimation task can be defined as:

$$\mathbf{X}_{DE}^I = \mathbf{H}[1, 1 : \tilde{K}, 1 : \tilde{N}_t] \quad (14a)$$

$$\mathbf{X}_{DE}^L = x_d. \quad (14b)$$

Similarly, \mathbf{X}_{PE}^I and \mathbf{X}_{PE}^L for path loss estimation task can be defined as:

$$\mathbf{X}_{PE}^I = \mathbf{H}[1, 1 : \tilde{K}, 1 : \tilde{N}_t] \quad (15a)$$

$$\mathbf{X}_{PE}^L = x_{pl}. \quad (15b)$$

IV. LLM FOR WIRELESS CHANNEL-ASSOCIATED TASKS

All of these tasks mentioned above are fundamentally rooted in the wireless channel, suggesting that multi-task learning can significantly enhance the model's ability to extract generalizable channel representations. This, in turn, would improve the performance of each individual task. To leverage this potential, we propose a multi-task method for wireless channel applications, empowered by LLM, which we refer to as LLM4WM. This approach integrates the learning of these tasks within a unified network framework based on LLM. Below, we provide a detailed overview of the network components and the training process for LLM4WM.

A. Preprocessor Module

Since the required channel characteristics for each task are different, a unified preprocessing approach is not conducive to

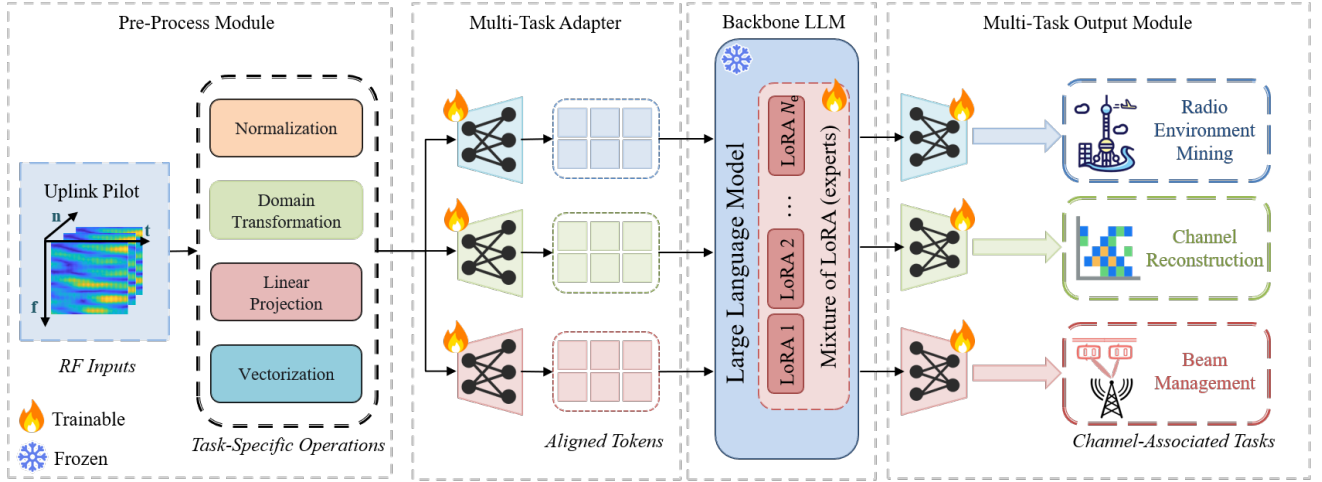


Fig. 2. The proposed LLM4WM is composed of four main modules: (i) pre-process module; (ii) multi-task adapter module; (iii) backbone LLM module fine-tuned with MoE-LoRA; (iv) multi-task output module

fully utilizing the unique characteristics of each task. Therefore, a corresponding preprocessing function is designed for each task to preprocess the input data, and the preprocessing process for the task n can be expressed as:

$$\mathbf{X}_n^{pre} = f_{pre,n}(\mathbf{X}_n^I), \quad (16)$$

where \mathbf{X}_n^{pre} denotes the preprocessed data, and $f_{pre,n}(\cdot)$ denotes the preprocessing operation for task t . Specifically, the preprocessing operation for the channel reconstruction tasks is tokenizing the CSI at each moment, that is, flattening the spatial and frequency features of the CSI as follows:

$$\mathbf{X}_n^{pre} = \text{Flatten}(\mathbf{X}_n^I, -2), \quad (17)$$

where the $\text{Flatten}(\mathbf{X}, i)$ operation denotes flattening the i -th dimension of the tensor \mathbf{X} and all subsequent dimensions into a single dimension. For tasks such as beamforming, distance estimation, and path loss estimation that require channel angle features, the CSI data will undergo domain transformation to convert the spatial domain CSI to angle domain CSI, i.e.,

$$\mathbf{X}_n^{pre} = \mathbf{X}_n^I \mathbf{F}_{\tilde{N}_n}, \quad (18)$$

where $\mathbf{F}_{\tilde{N}_t}$ is an \tilde{N}_t -dimensional DFT matrix.

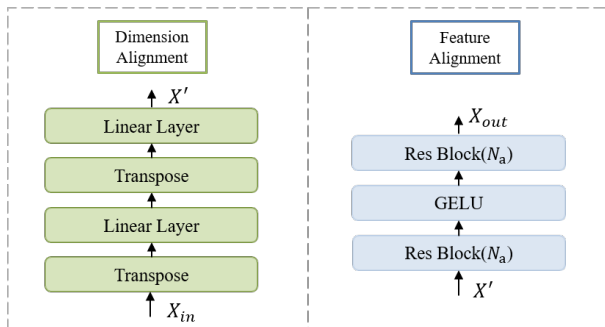


Fig. 3. An illustration of the multi-task adapter module.

B. Multi-Task Adapter Module

We extend the conventional use of adapter modules, which are small, trainable layers inserted between the layers of a pre-trained language model [27], [28]. This approach allows the model to maintain its existing modeling and generalization capabilities while adapting to a specific domain. However, it is primarily designed for single-task scenarios and lacks the ability to facilitate transfer generalization across multiple tasks simultaneously.

Unlike existing single-task adapters, the multi-task adapter modules function by parallelizing multiple individual adapters to simultaneously address various tasks. The features output by each adapter are then jointly fed into LLM for multi-task learning. This design fully leverages the generalization and multi-task learning capabilities of the LLM, while the joint adaptation approach also simplifies the training process of the network. Each individual adapter within the module is assigned to a specific task, performing task alignment and intrinsic representation alignment. As shown in Fig. 3, its main components include a linear alignment layer, residual feature extraction networks, and an activation function. In the individual adapter Adapter_n^{in} for task n , the linear alignment layer aims to align the semantic feature space and task feature space in terms of dimensions and get the feature map as:

$$\mathbf{X}_n^f = \text{Linear}(\mathbf{X}_n^{pre}) \in \mathbb{R}^{L \times D_{llm}}, \quad (19)$$

where L and D_{llm} denote the token length of the input to the LLM and the hidden layer dimension of the LLM, respectively. Since the preprocessed features are two-dimensional data, the $\text{Linear}(\cdot)$ operation includes at least two fully connected operations, which linearly map the first and second dimensions to the specified dimensions. Then the residual feature extraction networks and the activation function would act on \mathbf{X}_n^f to obtain feature maps with aligned semantic features as:

$$\mathbf{X}_n^a = \text{Res}(\text{GELU}(\text{Res}(\mathbf{X}_n^f))) \in \mathbb{R}^{L \times D_{llm}}, \quad (20)$$

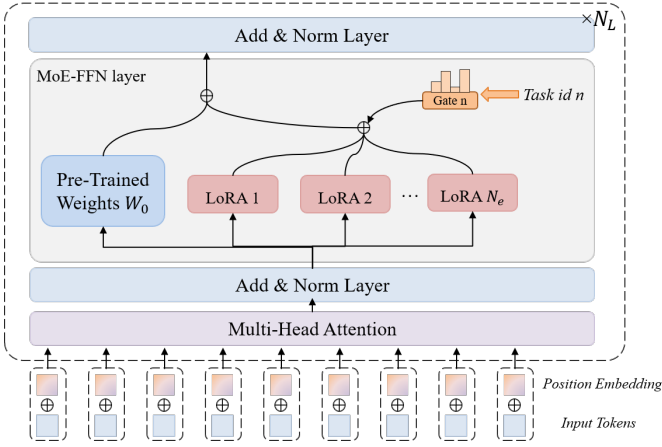


Fig. 4. An illustration of the MoE-LoRA fine-tuning method.

where the $\text{Res}(\cdot)$ operation includes $N_{a,i}$ Res-blocks. And each Res-block contains two 1-dimensional convolution kernels and an activation function $\text{ReLU}(\cdot)$. The convolution kernel size is 3, and the stride is 1. The $\text{GELU}(\cdot)$ function is a smooth, differentiable approximation of the $\text{ReLU}(\cdot)$ function [29]. The above steps can be simplified as:

$$\mathbf{X}_n^a = \text{Adapter}_n^{\text{in}}(\mathbf{X}_n^{\text{pre}}). \quad (21)$$

C. Mixture-of-LoRA Based Fine-tuning

The backbone LLM module is essential for processing the representations extracted by the adapters. To improve the pre-trained LLM's performance on wireless channel tasks, we efficiently fine-tune its parameters using MoE-LoRA, as shown in Fig. 4. This fine-tuning combines LoRA and MoE principles to enhance efficiency by selectively activating subsets of parameters. First, we outline the standard LoRA fine-tuning process, which trains two low-rank matrices in the model's feed-forward network and is tailored for single-task fine-tuning.

Assume the pre-trained weights are $W_0 \in \mathbb{R}^{d_{\text{out}} \times d_{\text{in}}}$, where d_{in} is the input dimension and d_{out} is the output dimension. The two trainable low-rank matrices are $A \in \mathbb{R}^{r \times d_{\text{in}}}$ and $B \in \mathbb{R}^{d_{\text{out}} \times r}$. Then, we can obtain the fine-tune weights $W \in \mathbb{R}^{d_{\text{out}} \times d_{\text{in}}}$ as follows:

$$W = W_0 + \frac{\alpha}{r}BA, \quad (22)$$

where r is the rank of the low-rank approximation. The hyperparameter α allows for adjusting the rank r and is typically set as $\alpha = 2 \times r$.

Assuming the input to the feed-forward network is x_t and the output is h_t , the forward propagation of the model can be expressed as follows:

$$h_t = Wx_t = W_0x_t + \frac{\alpha}{r}BAx_t. \quad (23)$$

To extend this concept to multi-task learning, we incorporate the well-known MoE models [30]. This approach establishes a collection of independent low-rank matrices that learn task-specific features individually. A gating network is then employed to select and combine different experts for various

tasks, facilitating a specific aggregation mechanism for the experts. The underlying idea is expressed as follows:

$$h_t = Wx_t = W_0x_t + \frac{\alpha}{r} \sum_{k=1}^{N_e} \omega_k B_k A_k x_t, \quad (24)$$

where $B_k \in \mathbb{R}^{d_{\text{out}} \times r}$ and $A_k \in \mathbb{R}^{r \times d_{\text{in}}}$ is the k -th pair of low-rank matrices. N_e and ω_k represents the number of experts and k -th experts' weights, respectively. A larger value of N_e indicates that more experts participate in the training and inference processes of the network. This can enhance the model's capacity for accurate representation. However, it also linearly increases the training and inference costs, meaning that the specific value of N_e requires a trade-off between model accuracy and inference speed.

Notably, the design of the gating network directly affects the performance of the MoE model. To avoid overfitting, we use a single-layer linear network to generate the expert weights for each task, and normalize the weight matrix using the $\text{Softmax}(\cdot)$ function to maintain the stability of the output data.

We apply MoE-LoRA to the linear layers within the feed-forward network (FFN) of LLM, while keeping the rest of the parameters frozen. This approach significantly reduces the number of tunable parameters in the model, greatly lowering training costs and improving training efficiency.

D. Multi-Task Output Module

Normal LLMs map the output features of transformer blocks to a probability distribution over the vocabulary, selecting the token with the highest probability as the output text. However, for wireless channel-associated tasks, the output is often challenging to express in text. Moreover, as the vocabulary size increases, this mapping incurs significant storage and computational costs. For instance, GPT-2's vocabulary of 50000 words necessitates an output layer with at least 50000 dimensions.

To address these challenges, and similar to the approach used in [31], we have designed a specific output layer tailored for wireless channel-associated tasks. This specialized output layer is intended to more effectively capture the target output relevant to these tasks, thereby improving performance and reducing the resource demands typically associated with large vocabulary sizes.

To align the task output with the LLM's semantic feature space, we use a multi-task adapter connected directly to the LLM's output, which is identical to the input adapter. Assuming the task n 's output feature of the large model is $\mathbf{X}_n^{\text{LLM}}$, and the multi-task adapter for the task n is denoted as $\text{Adapter}_n^{\text{out}}$, so this process can be represented as:

$$\mathbf{X}_n^p = \text{Adapter}_n^{\text{out}}(\mathbf{X}_n^{\text{LLM}}) \quad (25)$$

where \mathbf{X}_n^p denotes output of the multi-task adapter for task n .

Considering that channel estimation and channel prediction tasks are more sensitive to the learning of local features, we use CNNs for processing and dimensional alignment in subsequent steps. On the other hand, tasks such as beamforming, distance estimation, and path loss estimation require obtaining a global feature representation of the channel. Therefore, the

feature map will be flattened, and an MLP network will be employed for feature processing and dimensional alignment. The operations can be described as follows:

$$\mathbf{X}_n^o = \begin{cases} \text{CNN}(\mathbf{X}_n^p), & n \in \{CE, CP, PF\} \\ \text{MLP}(\mathbf{X}_n^p), & n \in \{BF, DE, PE\} \end{cases} \quad (26)$$

where \mathbf{X}_n^o represents prediction or estimation result of task n .

E. Training Configuration

The proposed network is trained on a multi-task mixed dataset using a two-stage training approach. In the first stage, only the multi-task adapters and output layer are trained, while the LLM parameters are frozen. At this point, the model learns the mapping between the task feature space and the pre-trained LLM's text feature space. In the second stage, the LLM is fine-tuned by MoE-LoRA, while the multi-task adapters become frozen, but the output layer is still trainable. At this stage, the model leverages the LLM for joint modeling of multiple tasks, achieving better results by utilizing generalized representations across tasks. The same loss function is used for both stages, as follows:

$$\text{Loss} = \sum_n \omega_n f_{\text{loss},n}(\mathbf{X}_n^o, \mathbf{X}_n^1) \quad (27)$$

where $f_{\text{loss},n}$ denotes the loss function for task n . And they are linearly combined with task weightings ω_n . To ensure that all tasks are well trained, we use the Dynamic Weight Average (DWA) algorithm [32] to dynamically adjust each task's weight based on its loss every epoch. The selection of loss function $f_{\text{loss},n}$ fully considers the characteristics of the task itself. For classification problems, such as *BF*, we use the cross entropy loss function, and for regression problems, such as *CP*, we use normalized mean square error (NMSE) [22] as the loss function.

V. EXPERIMENTS

In this section, we outline the simulation settings and subsequently evaluate the performance of the proposed LLM4WM method from several perspectives: overall performance, generalization ability, and stability. Comprehensive ablation experiments are also conducted to demonstrate the effectiveness of each module within the framework.

A. Simulation Setup

1) *Datasets*: We adopt the widely used channel generator QuaDRiGa [33] to simulate time-varying CSI datasets compliant with 3GPP standards. We consider a dual-frequency wireless system having a 1.9 GHz sub-6G link and a 28 GHz mmWave link. LOS propagation environment is assumed between BS and UEs such that the optimal transmitting beam for the mmWave link is determined by LOS direction. The hyper-parameters of the dataset generation are presented in Tab. II.

The sub-6G link operates in FDD mode to enhance spectrum utilization. Assuming that the uplink and downlink channels are adjacent, and for the uplink channel, a pilot is placed every

TABLE II
HYPER-PARAMETERS FOR DATASET GENERATION

Parameter	mmWave	sub-6G
Scenario	3GPP_38.901_UMa_LOS	
Active BSs	1	1
Codebook size B	256	N/A
Transmit antennas	64	8
Center frequency (GHz)	28	1.9
Bandwidth (GHz)	0.5	0.06
Antenna spacing	0.5	0.5
OFDM sub-carriers	64	64
Clusters	N/A	21
Paths per cluster	N/A	20

8 subcarriers. For the channel prediction task, we predict future $\tilde{P} = 4$ RBs based on historical $\tilde{T} = 16$ RBs and set the time interval of pilots as 0.5 ms, and for the frequency domain prediction task, the downlink channel at pilot is inferred from the uplink channel estimated or predicted by the uplink pilot.

In contrast, the mmWave link employs the TDD mode. For the sub-6G assisted mmWave beamforming task, the downlink analog precoding is also derived based on the spatial correlation of the uplink sub-6G channel estimated by the uplink pilot. The initial position of the user is randomized and the motion trajectory is set as linear type at a speed of 30 km/h. The dataset consists of 20000 samples, which are partitioned into a training set, validation set, and test set in a ratio of 9 : 1 : 2. Specifically, the training set contains 15000 samples, the validation set comprises 1600 samples, and the test set includes 3400 samples.

2) *Baselines*: To validate the superiority of the proposed method, several model-based and deep learning-based methods are implemented as baselines.

Traditional Methods (without deep learning): this class of methods does not rely on a training process but instead leverages the inherent characteristics of the channel to address specific problems.

- **BI**: In this method, CSI is treated as a time series and bilinear interpolation (BI) is used to complete the channel reconstruction tasks.
- **Codebook** [34]: Based on spatial correlation, a super-resolution codebook is used for beam scanning in the sub-6G band to obtain the optimal mmWave downlink beam vector. This method is used to process the beam management task.
- **FIFS** [35]: FIFS is a CSI-based fingerprinting system that presents a coherence bandwidth-enhanced probability algorithm with a correlation filter to map objects to the fingerprints. We implement it for the radio environment mining tasks.

Single-task Small Model Methods: This class of methods employs specially designed model components to address specific downstream tasks which often have a relatively small number of parameters.

- **MLP** [36], [37]: Multi-Layer Perceptron(MLP) is a type of feedforward neural network commonly used for classification and regression tasks. Many works have employed

MLPs to model complex mapping relationships in communication problems. We implement an MLP for the task of radio environment sensing and beam management.

- **LSTM** [38]: LSTM is designed with memory cells and multiplicative gates to deal with long-term dependency. We implement it using 4 LSTM layers for processing channel reconstruction tasks.
- **CNN** [23]: In [23], a CNN-based predictor is proposed for FDD systems, treating the prediction process of time-frequency CSI data as a two-dimensional image processing task. It contains ten convolutional layers, where the convolution kernel size is 3×3 . We implement it for processing channel reconstruction tasks.
- **WiT** [25]: A transformer-based location estimation method, which leverages the attention mechanism to achieve robust learning effects. We implement it as described in [25] for processing radio environment sensing tasks.
- **Transformer** [22]: In [22], a transformer-based parallel channel predictor is proposed for TDD systems to avoid error propagation problems. We implement it using 3 encoders and 2 decoders for processing channel reconstruction tasks.

Multi-Task Small Model Methods: This class of methods employs techniques such as low-level sharing and cross-feature fusion to enable feature sharing across different tasks, thereby achieving the functionality of a multi-purpose model.

- **Cross-stitch** [39]: A convolutional multi-task learning neural network equipped with “cross-stitch” unit, which could combine the activations from multiple networks. We implement it by using ResNet [40] as the backbone layer. To illustrate the impact of wireless multi-task learning for small model, **Cross-stitch(s)** is added as a baseline. We implement it by directly applying the cross-stitch network while only performing a single task.

Single-task Large Model Methods: This class of methods typically fine-tunes large models for a single downstream task, achieving strong performance by leveraging the powerful modeling capabilities of large models.

- **LLM4CP** [18]: This method is the first to apply the large language model to channel prediction task through fine-tuning. We implement it and choose gpt2 as the backbone LLM and LN Tuning [41] as the fine-tuning method for processing Channel Reconstruction tasks.
- **LLM4WM(s)**: A single-task fine-tuning based large model network, where we directly apply our proposed LLM4WM whilst only performing a single task.

3) *Network and Training Parameters:* In the simulation, we adopt the Multi-Task Adapter module with $N_a = 8$ for input and output feature alignment. For the configuration of the MoE-LoRA fine-tuning method, we choose the number of experts to be 8, as the number of experts is generally slightly greater than the number of tasks. Additionally, we set $r = 8$ for each LoRA matrix. For the output module, as mentioned above, for the specific task, we use either a three-layer MLP with 768-dimensional features or a three-layer CNN with 3×3 kernels for the feature process. and we employ only one single-

layer fully connected network to align the output dimensions. The smallest version [42] of GPT-2 with $F = 768$ feature dimension is adopted, the first $N_L = 6$ layers of which are deployed. Both the warm-up and cosine annealing scheduler are employed to train LLM4WM. The first 50 epochs serve as the warm-up phase, where the learning rate increases linearly from the minimum value of 1×10^{-5} to 1×10^{-3} . In the subsequent training phases, the learning rate is dynamically adjusted using the cosine annealing scheduler. Several other hyper-parameters for model training are illustrated in Tab. III.

TABLE III
HYPER-PARAMETERS FOR NETWORK TRAINING

Parameter	Value
Batch size	512
Epochs	250
Optimizer	Adam (betas=(0.9, 0.999))
Learning rate scheduler	Cosine Annealing
Cosine annealing period	100 epochs
Learning rate range	$[1 \times 10^{-5}, 1 \times 10^{-3}]$

4) *Performance Metric:* To evaluate performance, we employ task-specific metrics. For channel reconstruction tasks, we measure the NMSE between predictions and ground truth. The beam management task utilizes the Top-1 accuracy which shows the frequency of whether the model correctly predicts the beam index, and distance estimation and path loss estimation rely on mean absolute error (MAE) and NMSE, respectively. Meanwhile, we calculated the average metric Avg. across all tasks for each model to facilitate intuitive comparisons. The calculation of this average metric is as follows:

$$\text{Avg.} = \frac{1}{6} * [\text{NMSE (CE)} + \text{NMSE (CP)} + \text{NMSE (PF)} + (1 - \text{Acc (BF)}) + \text{MAE (DE)} + \text{NMSE (PE)}]. \quad (28)$$

In order to comprehensively evaluate the performance of the proposed scheme, we adopt an extra metrics, namely SE which reflect the performance of the communication system. SE is an important metric that reveals the achievable rate of the system, reflecting the effectiveness of communication. It is calculated by Eq. (4), where $\mathbf{h}_{t,k}$ is the actual CSI and \mathbf{w}_t is obtained as Eq. (7) with predicted $\mathbf{h}_{t,k}$. The communication SNR is defined as $1/\sigma_n^2$ and set as 10 dB.

B. Performance Evaluation

1) *Overall Performance:* Tab. IV shows that LLM4WM outperforms non-learning methods, small models, and single-task fine-tuning across various tasks. Its success stems from leveraging the general knowledge of pre-trained large language models and its multi-task learning capability, which enhances feature representation. In contrast, single-task fine-tuning is prone to overfitting, leading to performance degradation in challenging scenarios. LLM4WM’s combination of a Multi-Task Adapter and MoE-LoRA aligns feature spaces across tasks, resulting in more generalized performance. Our analysis of multi-task learning on large models (LM) and small

TABLE IV
PERFORMANCE OF LLM4WM AND OTHER BASELINES: FOR MMWAVE LINK, THE MAXIMUM SE IS $9.32 \text{ BIT} \cdot (\text{s} \cdot \text{Hz})^{-1}$; FOR SUB-6G LINK, THE MAXIMUM SE IS $6.33 \text{ BIT} \cdot (\text{s} \cdot \text{Hz})^{-1}$. THE BEST RESULTS ARE HIGHLIGHTED IN **BOLD**, WHILE THE SECOND-BEST RESULTS ARE UNDERLINED.

Method	CE		CP		PF		Method	BF		Method	DE	PE	Avg. ↓
	NMSE ↓	SE ↑	NMSE ↓	SE ↑	NMSE ↓	SE ↑		Acc ↑	SE ↑		MAE ↓	NMSE ↓	
BI	0.654	5.612	1.796	2.965	1.293	5.321	Codebook	0.288	7.868	FIFS	0.249	0.204	0.818
CNN	0.119	6.043	0.125	6.038	0.283	5.888	CNN	0.356	6.852	WiT	0.160	0.053	0.230
LSTM	1.000	4.182	0.161	5.994	0.280	5.902	MLP	0.831	8.522	MLP	0.218	0.091	0.320
Cross-stitch(s)	0.153	5.999	0.112	6.058	0.226	5.947	Cross-stitch(s)	<u>0.884</u>	<u>8.545</u>	Cross-stitch(s)	0.177	0.054	0.140
Cross-stitch	0.157	5.996	0.112	6.059	0.232	5.947	Cross-Stitch	0.858	8.525	Cross-stitch	<u>0.131</u>	<u>0.032</u>	0.134
LLM4CP	<u>0.106</u>	<u>6.062</u>	<u>0.106</u>	<u>6.066</u>	0.151	6.027	LLM4CP	0.682	8.430	LLM4CP	0.199	0.122	0.167
LLM4WM(s)	0.108	6.060	0.106	6.057	<u>0.114</u>	<u>6.061</u>	LLM4WM(s)	0.878	8.530	LLM4WM(s)	0.153	0.052	<u>0.109</u>
LLM4WM	0.103	6.069	0.106	6.068	0.100	6.081	LLM4WM	0.904	8.557	LLM4WM	0.087	0.028	0.087

models (SM) reveals that the small model suffers an average improvement of only 0.19 dB when switching from single-task to multi-task learning, while the large model shows an improvement of 0.99 dB. This is due to the large model's ability to extract joint representations, unlike the small model, which struggles with conflicting task knowledge. Thus, large models are better suited for handling multiple downstream tasks.

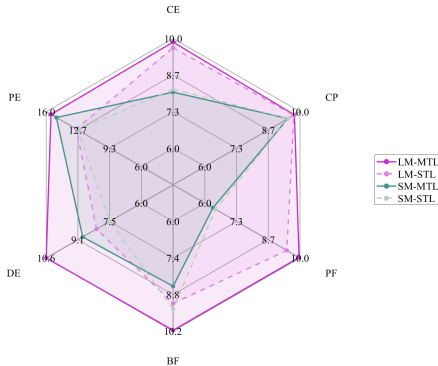


Fig. 5. Performance comparison of large and small models before and after wireless multi-task learning.

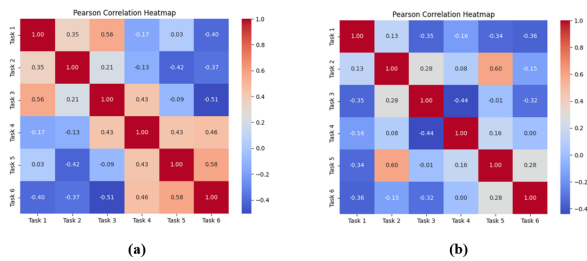


Fig. 6. Pearson correlation coefficient heatmap of expert combination weights for various tasks

To verify whether the experts in the MoE are effectively allocated based on task types, we use the Pearson correlation coefficient as a metric. Heatmaps of expert combinations weights from two randomly selected MoE-LoRA layers are shown in Fig. 6. The results reveal that the correlation be-

tween expert combination weights for most tasks is quite low, indicating that the gating network indeed learns distinct expert combinations for different task types. Additionally, it can be observed that tasks with similar characteristics exhibit higher correlations, likely due to the fact that neighboring tasks often belong to the same task set, thus exhibiting stronger correlations.

2) *Generalization Experiments*: Generalization is the model's ability to maintain performance in new communication scenarios, crucial for real-world deployment as it reduces the need for frequent updates. We use only 10% of the RMa dataset to transfer a model trained in the UMa scenario, as well as a model trained on the 1.9 GHz sub-6 GHz link dataset to the 2.4 GHz sub-6 GHz link dataset. Results in Tab. V indicate that, despite the challenges of multi-task generalization and transfer, our approach consistently outperforms others across most tasks. The slight dip in radio environment mining performance is due to the task's relative simplicity in the LOS scenario, where smaller models like WiT excel. However, our model excels in more complex tasks like channel estimation, which requires understanding multidimensional features, further confirming that large models are better suited for dynamic real-world communication scenarios.

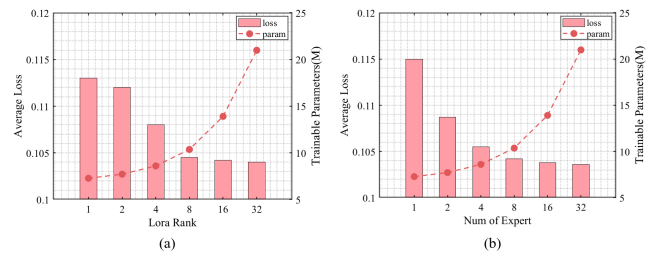


Fig. 7. The performance of LLM4WM under different Lora ranks and number of experts.

3) *Hyper-parameter Analysis*: To illustrate the rationale behind the hyperparameter settings, we conduct a thorough experiment into the impact of hyperparameters on the performance of LLM4WM. Specifically, we examine the effects of varying the LoRA rank and the number of experts, as depicted in Fig. 7. When we increase the LoRA rank while keeping the number of experts fixed at 8, the performance of LLM4WM

TABLE V

GENERALIZATION PERFORMANCE OF LLM4WM AND OTHER BASELINES: THE AVERAGE LOSS ACROSS TASKS IS COMPUTED AND PRESENTED IN THE FINAL COLUMN LABELED "AVG.". THE BEST RESULTS ARE HIGHLIGHTED IN **BOLD**, WHILE THE SECOND-BEST RESULTS ARE UNDERLINED.

Train Set	Test Set	Method	CE	CP	PF	Method	BF	Method	DE	PE	Avg. ↓
			NMSE ↓	NMSE ↓	NMSE ↓		Acc ↑		MAE ↓	NMSE ↓	
UMa 1.9GHz	RMa 1.9GHz	LLM4WM	0.143	<u>0.145</u>	0.162	LLM4WM	0.413	LLM4WM	0.336	<u>0.285</u>	0.276
		LLM4CP	<u>0.177</u>	0.133	<u>0.292</u>	LLM4CP	0.306	LLM4CP	0.370	0.311	<u>0.330</u>
		CNN	0.187	0.137	0.384	CNN	0.215	WiT	<u>0.339</u>	0.220	0.376
	LSTM	1.000	0.309	0.545	MLP	<u>0.365</u>	MLP	0.539	0.473	0.584	
	UMa 2.4GHz	LLM4WM	0.101	0.110	0.135	LLM4WM	0.785	LLM4WM	0.126	0.047	0.122
		LLM4CP	<u>0.110</u>	<u>0.113</u>	<u>0.196</u>	LLM4CP	0.685	LLM4CP	0.182	0.073	<u>0.165</u>
		CNN	0.115	0.121	0.381	CNN	0.375	WiT	<u>0.143</u>	<u>0.047</u>	0.239
		LSTM	1.000	0.174	0.340	MLP	<u>0.769</u>	MLP	0.256	0.134	0.356

TABLE VI

TEST RESULTS OF ABLATION EXPERIMENTS FOR MULTI-TASK ADAPTER MODULE AND THE BACKBONE LLM MODULE.

Metric	LLM4WM	w/o Adapter _{in}	w/o Adapter _{out}	w/o Adapter	w/o LLM	Frozen LLM
Average Loss	0.087	0.092	0.095	0.102	0.117	0.092
Loss Increase Ratio	0.00%	6.50%	9.54%	17.62%	34.40%	6.15%

gradually improves. This can be attributed to the enhanced adaptability of the model to the data distribution due to the increase in trainable parameters. However, this improvement comes at the cost of increased training overhead. After weighing the trade-off between performance and computational cost, we determine that a LoRA rank of 8 provided the optimal balance. Subsequently, with the LoRA rank fixed at its optimal value of 8, we incrementally increase the number of experts. A similar trend to that of the LoRA rank was observed, as an increase in the number of experts effectively enhanced the model’s analytical and representational capacity. Balancing performance and computational efficiency, we determine that setting the number of experts to 8 was the most appropriate choice.

4) *Ablation Experiments:* To validate the proposed modules, we conducted ablation experiments by removing or altering configurations of the multi-task adapter and backbone LLM modules. Variations for the multi-task adapter include w/o Adapter_{in} (placing adapter only on the output side of the LLM), w/o Adapter_{out} (placing adapter only on the input side of the LLM), and w/o Adapter (no adapters). For the backbone LLM, variations include w/o LLM (removing the large model) and frozen LLM (freezing pre-trained weights). Results in Table V show that all ablation configurations led to performance declines, highlighting the effectiveness of both the multi-task adapter and backbone LLM modules. Notably, the impact of removing the backbone LLM is significantly greater, indicating its critical role in the success of multi-task joint learning for wireless tasks.

5) *Efficiency Evaluation:* We compare the model training and inference cost of the proposed method with other baselines to assess the difficulty of deploying the model in practical scenarios, as shown in Tab. VII. All experiments are conducted on the same machine with 4 Intel Xeon Platinum 8375C CPUs, 4 NVIDIA GeForce RTX4090 GPUs, and 256 GB of RAM. To facilitate representation and comparison, the data

in the table reflects the average performance across tasks for each method. Notably, the MoE-LoRA fine-tuning method results in LLM4WM having trainable parameters comparable to those of smaller models. This highlights both the training efficiency and parameter efficiency of LLM4WM, as adding new tasks increases the model’s parameters by only about 1.13 M, a small fraction of the total. Additionally, utilizing a lightweight backbone LLM ensures that the overall inference speed of LLM4WM remains acceptable. Thus, LLM4WM demonstrates significant potential for deployment in future communication scenarios marked by increasing demand and the need for customized services involving numerous tasks.

VI. CONCLUSIONS

In this paper, we have proposed a novel multi-task fine-tuning framework tailored for large models in wireless communication systems. By leveraging a diverse multi-task dataset, our approach has enabled the model to perform various wireless channel-associated tasks concurrently. To facilitate the extraction of shared representations across multiple tasks, we integrated MoE-LoRA into the fine-tuning process, empowering the backbone model to dynamically adapt by optimally combining expert modules and improving task-specific performance. Additionally, we employed a multi-task adapter to harmonize the feature spaces of different tasks with the semantic embedding space of the large model, ensuring coherent task alignment. Preliminary simulation results have demonstrated the robust multi-task learning and generalization capabilities of the proposed LLM4WM framework. Furthermore, ablation studies have underscored the critical contributions of each module to overall system performance. The expert weight heatmap has validated the efficacy of the MoE mechanism in adaptively allocating expert resources, highlighting its role in enhancing model specialization and flexibility.

TABLE VII
NETWORK PARAMETERS (TRAINABLE PARAMETERS/TOTAL PARAMETERS) AND THE INTERFERENCE COST PER BATCH.

Metric	MLP	CNN	LSTM	WIT	LLM4CP	LLM4WM
Trainable Network parameters (M)	1.29	2.14	1.17	19.19	1.80	1.13
Total Network parameters (M)	1.29	2.14	1.17	19.19	82.91	88.71
Interference time (ms)	0.32	0.49	6.49	2.97	8.62	6.00

REFERENCES

- [1] E. G. Larsson, O. Edfors, F. Tufvesson, and T. L. Marzetta, "Massive MIMO for Next Generation Wireless Systems," *IEEE Commun. Mag.*, vol. 52, no. 2, pp. 186–195, Feb. 2014.
- [2] L. Lu, G. Y. Li, A. L. Swindlehurst, A. Ashikhmin, and R. Zhang, "An Overview of Massive MIMO: Benefits and Challenges," *IEEE J. Sel. Top. Signal Process.*, vol. 8, no. 5, pp. 742–758, Apr. 2014.
- [3] F. Rusek *et al.*, "Scaling Up MIMO: Opportunities and Challenges with Very Large Arrays," *IEEE Signal Process. Mag.*, vol. 30, no. 1, pp. 40–60, Jan. 2012.
- [4] S. Gao, X. Cheng, and L. Yang, "Estimating Doubly-Selective Channels for Hybrid mmWave Massive MIMO Systems: A Doubly-Sparse Approach," *IEEE Trans. Wireless Commun.*, vol. 19, no. 9, pp. 5703–5715, May 2020.
- [5] M. Soltani, V. Pourahmadi, A. Mirzaei, and H. Sheikhzadeh, "Deep Learning-Based Channel Estimation," *IEEE Commun. Lett.*, vol. 23, no. 4, pp. 652–655, Feb. 2019.
- [6] E. Balevi, A. Doshi, A. Jalal, A. Dimakis, and J. G. Andrews, "High Dimensional Channel Estimation Using Deep Generative Networks," *IEEE J. Sel. Areas Commun.*, vol. 39, no. 1, pp. 18–30, Nov. 2020.
- [7] M. Arvinte and J. I. Tamir, "MIMO Channel Estimation Using Score-Based Generative Models," *IEEE Trans. Wireless Commun.*, vol. 22, no. 6, pp. 3698–3713, Nov. 2022.
- [8] X. Cheng *et al.*, "Intelligent Multi-Modal Sensing-Communication Integration: Synesthesia of Machines," *IEEE Commun. Surv. Tutorials*, Nov. 2023.
- [9] H. Zhang, S. Gao, X. Cheng, and L. Yang, "Integrated Sensing and Communications Towards Proactive Beamforming in mmWave V2I via Multi-Modal Feature Fusion (MMFF)," *IEEE Trans. Wireless Commun.*, June 2024.
- [10] Z. Yang, S. Gao, X. Cheng, and L. Yang, "Synesthesia of Machines (SoM)-Enhanced ISAC Precoding for Vehicular Networks with Double Dynamics," *arXiv preprint arXiv:2408.13546*, Dec. 2024.
- [11] A. Jagannath and J. Jagannath, "Multi-task Learning Approach for Automatic Modulation and Wireless Signal Classification," in *IEEE Int. Conf. Commun. (ICC)*, June 2021, pp. 1–7.
- [12] W. Xie, J. Xiao, P. Zhu, and C. Yu, "Multi-Task Learning-Based Channel Estimation for RIS Assisted Multi-User Communication Systems," *IEEE Commun. Lett.*, vol. 26, no. 3, pp. 577–581, Dec. 2021.
- [13] T. Brown *et al.*, "Language Models are Few-Shot Learners," *Adv. Neural Inf. Process. Syst.*, vol. 33, pp. 1877–1901, Dec. 2020.
- [14] K. Singhal *et al.*, "Towards Expert-Level Medical Question Answering with Large Language Models," *arXiv preprint arXiv:2305.09617*, May 2023.
- [15] P. Colombo *et al.*, "SaulLM-7B: A Pioneering Large Language Model for Law," *arXiv preprint arXiv:2403.03883*, Mar. 2024.
- [16] S. Wu *et al.*, "BloombergGPT: A Large Language Model for Finance," *arXiv preprint arXiv:2303.17564*, Dec. 2023.
- [17] Z. Peng, L. Dong, H. Bao, Q. Ye, and F. Wei, "BEiT v2: Masked Image Modeling with Vector-Quantized Visual Tokenizers," *arXiv preprint arXiv:2208.06366*, Oct. 2022.
- [18] B. Liu, X. Liu, S. Gao, X. Cheng, and L. Yang, "LLM4CP: Adapting Large Language Models for Channel Prediction," *J. Commun. Inf. Networks*, vol. 9, no. 2, pp. 113–125, June 2024.
- [19] B. Liu, S. Gao, X. Liu, X. Cheng, and L. Yang, "WiFo: Wireless Foundation Model for Channel Prediction," *arXiv preprint arXiv:2412.08908*, Dec. 2024.
- [20] Q. Liu *et al.*, "When MOE Meets LLMs: Parameter Efficient Fine-tuning for Multi-task Medical Applications," in *Proc. Int. ACM SIGIR Conf. Res. Dev. Inf. Retr. (SIGIR)*, Washington D.C., USA, July 2024, pp. 1104–1114.
- [21] T. L. Marzetta, E. G. Larsson, H. Yang, and H. Q. Ngo, *Fundamentals of Massive MIMO*. Cambridge University Press, 2016.
- [22] H. Jiang, M. Cui, D. W. K. Ng, and L. Dai, "Accurate Channel Prediction Based on Transformer: Making Mobility Negligible," *IEEE J. Sel. Areas Commun.*, vol. 40, no. 9, pp. 2717–2732, July 2022.
- [23] M. S. Safari, V. Pourahmadi, and S. Sodagari, "Deep UL2DL: Data-Driven Channel Knowledge Transfer From Uplink to Downlink," *IEEE Open J. Veh. Technol.*, vol. 1, pp. 29–44, Dec. 2019.
- [24] S. Lv, X. Li, J. Liu, and M. Shi, "Sub-6G Aided Millimeter Wave Hybrid Beamforming: A Two-Stage Deep Learning Framework With Statistical Channel Information," *IEEE Trans. Green Commun. Networking*, Jan. 2024.
- [25] A. Salihu, S. Schwarz, and M. Rupp, "Attention Aided CSI Wireless Localization," in *IEEE Workshop Signal Process. Adv. Wireless Commun. (SPAWC)*, Oulu, Finland, July 2022, pp. 1–5.
- [26] Y. Sun *et al.*, "Environment Features-Based Model for Path Loss Prediction," *IEEE Wireless Commun. Lett.*, vol. 11, no. 9, pp. 2010–2014, July 2022.
- [27] Y.-L. Sung, J. Cho, and M. Bansal, "VL-Adapter: Parameter-Efficient Transfer Learning for Vision-and-Language Tasks," in *IEEE Conf. Comput. Vis. Pattern Recognit. (CVPR)*, New Orleans, LA, USA, June 2022, pp. 5227–5237.
- [28] J. Pan, Z. Lin, X. Zhu, J. Shao, and H. Li, "ST-Adapter: Parameter-Efficient Image-to-Video Transfer Learning," *Adv. Neural Inf. Process. Syst.*, vol. 35, pp. 26462–26477, Nov. 2022.
- [29] D. Hendrycks and K. Gimpel, "Gaussian Error Linear Units (GELUs)," *arXiv preprint arXiv:1606.08415*, June 2016.
- [30] N. Shazeer *et al.*, "Outrageously Large Neural Networks: The Sparsely-Gated Mixture-of-Experts Layer," *arXiv preprint arXiv:1701.06538*, Jan. 2017.
- [31] D. Wu *et al.*, "NetLLM: Adapting Large Language Models for Networking," in *Proc. ACM SIGCOMM Conf. (SIGCOMM)*, Sydney, NSW, Australia, Aug. 2024, pp. 661–678.
- [32] S. Liu, E. Johns, and A. J. Davison, "End-to-End Multi-Task Learning with Attention," in *IEEE Conf. Comput. Vis. Pattern Recognit. (CVPR)*, Long Beach, CA, USA, June 2019, pp. 1871–1880.
- [33] S. Jaeckel, L. Raschkowski, K. Börner, and L. Thiele, "QuADriGa: A 3-D Multi-Cell Channel Model With Time Evolution for Enabling Virtual Field Trials," *IEEE Trans. Antennas Propag.*, vol. 62, no. 6, pp. 3242–3256, Mar. 2014.
- [34] A. Ali, N. González-Prelcic, and R. W. Heath, "Millimeter Wave Beam-Selection Using Out-of-Band Spatial Information," *IEEE Trans. Wireless Commun.*, vol. 17, no. 2, pp. 1038–1052, Nov. 2017.
- [35] J. Xiao, K. Wu, Y. Yi, and L. M. Ni, "FIFS: Fine-Grained Indoor Fingerprinting System," in *Proc Int Conf Comput Commun Networks (ICCCN)*, Munich, Germany, July 2012, pp. 1–7.
- [36] M. Alrabeiah and A. Alkhateeb, "Deep Learning for mmWave Beam and Blockage Prediction Using Sub-6 GHz Channels," *IEEE Trans. Commun.*, vol. 68, no. 9, pp. 5504–5518, June 2020.
- [37] P. Ferrand, A. Decurninge, and M. Guillaud, "DNN-based Localization from Channel Estimates: Feature Design and Experimental Results," in *IEEE Glob. Commun. Conf. (GLOBECOM)*, Taipei, Taiwan, Dec. 2020, pp. 1–6.
- [38] W. Jiang and H. D. Schotten, "Deep Learning for Fading Channel Prediction," *IEEE Open J. Commun. Soc.*, vol. 1, pp. 320–332, Mar. 2020.
- [39] I. Misra, A. Shrivastava, A. Gupta, and M. Hebert, "Cross-stitch networks for multi-task learning," in *IEEE Conf. Comput. Vis. Pattern Recognit. (CVPR)*, Las Vegas, Nevada, June 2016, pp. 3994–4003.
- [40] K. He, X. Zhang, S. Ren, and J. Sun, "Deep Residual Learning for Image Recognition," in *IEEE Conf. Comput. Vis. Pattern Recognit. (CVPR)*, Las Vegas, NV, USA, June 2016, pp. 770–778.
- [41] W. Qi, Y.-P. Ruan, Y. Zuo, and T. Li, "Parameter-Efficient Tuning on Layer Normalization for Pre-trained Language Models," *arXiv preprint arXiv:2211.08682*, Dec. 2022.
- [42] A. Vaswani, "Attention Is All You Need," *Adv. Neural Inf. Process. Syst.*, Dec. 2017.